RESEARCH ARTICLE

Cascade PID Control Systems Based on DNA Strand Displacement With Application in Polarization of Tumor-Associated Macrophages

HUIHUI XUE[1], HUI LV[1,2], YIJUN XIAO[1], AND XING'AN WANG[3,4]
[1]Key Laboratory of Advanced Design and Intelligent Computing, Ministry of Education, School of Software Engineering, Dalian University, Dalian, Liaoning 116622, China
[2]State Key Laboratory of Synthetical Automation for Process Industries, Northeastern University, Shenyang, Liaoning 110004, China
[3]College of Environmental and Chemical Engineering, Dalian University, Dalian, Liaoning 116622, China
[4]Dalian Chivy Biotechnology Company Ltd., Dalian, Liaoning 116023, China
Corresponding author: Hui Lv (lh8481@tom.com)

ABSTRACT Disturbances are widespread in biochemical systems. Nowadays, prevalent single-loop control strategies only take external disturbances into account. However, internal perturbations that threaten the stability of biochemical systems are invariably ignored. In this paper, a DNA strand displacement (DSD)-based cascade PID control system is designed. In addition to traditionally realizing the tracking of reference input and the attenuation of primary disturbance, the presented control approach also innovatively completes the rejection of secondary disturbance. Specifically, the dynamics of the reference input signal are first governed by a first-order low-pass filter integrated with cascade PID control systems, which efficiently avoids the excessive response of the cascaded primary and secondary controllers to the reference signal. Then, cascade PID controllers and second-order time-delay plants are constructed by utilizing the chemical reaction network (CRN) and the DSD. In terms of secondary perturbation suppression, the obtained control scheme significantly outperforms the single-loop PID control scheme with a smaller overshoot and faster settling time. Finally, the DSD-based cascade PID control method is applied to regulate gene expressions of interferon regulatory factor 4 (IRF4) and interferon regulatory factor 5 (IRF5) that affect the polarization of tumor-associated macrophages (TAMs). Compared with the single-loop PID control strategy, the cascade PID control strategy exhibits a better inhibitory effect on IRF5 gene overexpression (internal disturbance) and TAMs endogenous gene expression (external disturbance).

INDEX TERMS Cascade PID control systems, chemical reaction networks, DNA strand displacement, secondary disturbance, regulation of tumor-associated macrophage polarization.

I. INTRODUCTION

Due to some natural properties (e.g., variability and nonlinearity) [1], biochemical systems have difficulty in gaining

The associate editor coordinating the review of this manuscript and approving it for publication was Valentina E. Balas.

a predetermined behavior, which hinders the further application of synthetic biology [2] in various fields. In order to obtain a stable and robust biochemical system, it is essential to build control systems in the form of biomolecular circuits [3], [4]. Unlike traditional computing methods, biomolecular circuits are able to operate in wet environments and interact with mammalian cells [5].

As an essential intermediate abstraction layer, a chemical reaction network (CRN) [6], [7] can be used to accomplish the mapping from a biomolecular circuit to a control system. Initially, Oishi et al. [8] proposed a CRN design strategy for the basic modules of a linear control system that include integral, gain, and summation. A further investigation [9] proved that the quasi-sliding mode controller, a nonlinear controller, could be realized by the chemical reaction networks (CRNs) via unimolecular and bimolecular reactions. In addition, Paulino et al. [10] and Whitby et al. [11] presented the CRN design methods for PID controllers widely used in control systems. Once the CRN of the control system is successfully constructed, the biomolecular reaction network corresponding to the CRN is no longer impossible for us to design.

DNA strand displacement (DSD) reactions [12], [13] with programmability are taken into account for realizing the CRN-based control systems. In recent years, an increasing number of control systems based on DNA strand displacement have been developed, such as PI [8], PID [10], [11], state feedback [10], [14], static pre-filters [14], and two-degree-of-freedom (2-DOF) PID control systems [15], [16]. First, Oishi et al. [8] proposed the DSD design strategies for three fundamental chemical reactions (i.e., catalytic, degradation, and annihilation reactions) that make up the CRN of PI control systems. Next, Paulino et al. [10] constructed first-order time-delay plants and PID control methods based on DSD by utilizing the Padé approximation. Furthermore, the singular perturbation theory was applied to design the DSD reactions of PID feedback control systems [11]. Then Yuan et al. [15] used DSD to build a 2-DOF PID controller for restraining primary disturbance. Subsequently, the DSD technology was adopted to establish state feedback controllers and static pre-filters [14], which stabilized the divergent linear time-invariant system.

So far, the DSD-based control strategies have focused on set-point tracking and external disturbance suppression. However, the ubiquitous internal perturbations in biochemical systems have been neglected, which makes it hard to obtain sufficiently good performance for synthetic biochemical circuits. By introducing a feedback loop, the cascade control system [17] exhibits an efficient and robust control effect against secondary disturbances. The system is suitable for a variety of controlled process models, including nonlinear processes [18], stable processes [19], time-delay processes [20], [21], and others. For a stable second-order time-delay process, this paper uses the controller parameter tuning method proposed by Siddiqui et al. [19] to determine the parameters of the cascade PID controller. In the last few years, cascade control structures have been widely applied in mechanical equipment [22], [23], air systems [24], and chemical processes [25]. But the control methods have not been put to use in regulating biochemical systems.

Several control strategies have stabilized complex biochemical systems in prior studies, such as gene regulatory devices [11], [26], genetic control systems [27], and small RNA-based negative feedback circuits [28]. However, there are no control methods for regulating the polarization of tumor-associated macrophages (TAMs). TAMs [29], [30] are one of the main targets of cancer immunotherapy. While the interferon regulatory factor 5 (IRF5) gene is heavily activated, the TAMs are polarized into M1-type macrophages to kill tumor cells. If the interferon regulatory factor 4 (IRF4) gene is predominantly expressed, the TAMs polarize into M2-type macrophages contributing to tumor growth. It has been experimentally demonstrated that IRF4 and IRF5 are up-regulated by miR125a [31] and miR125b [32], respectively, which provides an interface for the regulation of tumor-associated macrophage polarization. Therefore, it is feasible and necessary to control the above-mentioned gene expression process by biochemical controllers like a cascade PID controller, when endogenous gene expression and gene overexpression result in IRF4 and IRF5 gene expression not reaching the desired level.

Based on chemical reaction networks, cascade PID control methods are designed for second-order biochemical plants with time delay and internal disturbance. Due to the ease of programming, DSD reactions are specially selected to realize the CRNs of cascade PID controllers. First, a first-order low-pass filter is incorporated into a cascade PID control scheme to limit the dynamics of a reference input signal, which reduces the control signal received from the cascaded controller and the overshoot responding to the reference signal. Second, the manuscript presents CRNs-based cascade PID control strategies that are characterized by the feedback loop contained in a closed loop. To integrate with the control strategies, second order plus time delay (SOPTD) plants are established by using CRNs. Furthermore, the cascade PID control systems are equivalently mapped in DSD reaction networks by the above CRNs. The cascade PID control approaches expressed by the CRN and DSD exhibit an effective and superior suppression for secondary disturbances. Third, gene overexpression (internal disturbance) and endogenous gene expression (external disturbance) affect the transcriptional regulatory processes and gene expression levels of IRF4 and IRF5 in TAMs, respectively. By placing the transcription and translation processes in the secondary and primary loops separately, IRF4 and IRF5 gene expressions are regulated by a DSD-based cascade PID control approach. It is worth noting that the gene expression processes of IRF4 and IRF5 combined with the cascade PID controller remain under control during disturbances.

The contributions of this paper are as follows: (1) Cascade PID control strategies and stable second-order time delay plants are constructed by utilizing CRN and DSD. With regard to tracking the set point and attenuating the secondary disturbance, the proposed control system performs better than the single-loop PID control system. (2) A first-order low-pass filter is employed for adjusting the dynamic of the reference signal in cascade PID control systems, which avoids the
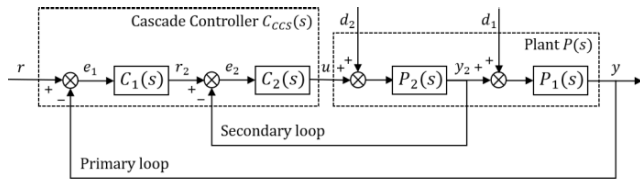
FIGURE 1. Structure of cascade control system Σ_{CCS}.

unnecessary overshoot of control systems and the excessive consumption of DNA species caused by tracking the reference input. (3) To control the polarization process of TAMs, a cascade PID control approach based on DSD technology is applied to IRF4 and IRF5 gene expression regulation. The control method can timely remove the impact of gene overexpression on the transcription level and endogenous gene expression on the translation level.

The rest of this paper is organized as follows. Section II aims at designing a cascade PID control system, which shows in detail the design and improvement of the cascade PID controller. In Section III, a CRNs-based cascade PID control system is successfully constructed and verified in Visual DSD. Using the obtained CRN, the DSD of the cascade PID controller is built and simulated in Section IV. Section V considers the application of a DSD-based cascade PID control strategy to regulate the polarization of tumor-associated macrophages, along with a comparison to a single-loop PID control system. Finally, Section VI provides the conclusion of this paper.

II. CASCADE PID CONTROL SYSTEMS
The section aims to design and improve cascade control systems that the CRN and DSD are expected to implement. First, the parameters of cascade controller are determined by the plants and reference models of the primary and secondary loops. Then, a low-pass filter follows the reference input of a cascade PID control system to prevent primary and secondary controllers in series from accumulatively amplifying the input signal. Additionally, Matlab is used to confirm that the filter is available for diminishing the system overshoot and controller output.

A. DESIGN OF CASCADE PID CONTROL SYSTEMS
A primary loop and a secondary loop make up the cascade control system (CCS) shown in Fig. 1, where the secondary loop is embedded in the primary loop. The secondary loop, also known as the inner loop, is composed of the secondary controller $C_2(s)$ and secondary process $P_2(s)$. The primary loop is referred to as the outer loop as well, which includes the primary controller $C_1(s)$ and the primary process $P_1(s)$. The plant $P(s)$ controlled by the cascade PID controller $C_{CCS}(s)$ is separated into $P_1(s)$ and $P_2(s)$. r_2, e_2, and y_2 represent the reference signal, error signal, and output signal of the inner loop. In the outer loop, the reference signal, error signal, and output signal are labeled by r, e_1, and y. d_1 and d_2 are the

primary disturbance and secondary disturbance suffered by the object $P_1(s)$ and $P_2(s)$, respectively. Note that the signals in the cascade control system are functions of time rather than constants. For simplicity, the time dependence of functions is omitted, taking the example that $r(t)$ is replaced by r.

According to the Mason's gain formula, a series of transfer functions for the cascade PID control system Σ_{CCS} is derived from the signal flow graph (Fig. 1). In the secondary loop, the transfer function from r_2 to y_2 is given as

$$F_{y_2 r_2}(s) = \frac{C_2(s) P_2(s)}{1 + C_2(s) P_2(s)} \quad (1)$$

The transfer function of the primary loop, from r to y, is obtained by

$$F_{yr}(s) = \frac{C_1(s)C_2(s)P_1(s)P_2(s)}{1 + C_2(s)P_2(s) + C_1(s)C_2(s)P_1(s)P_2(s)} \quad (2)$$

In the cascade PID control system Σ_{CCS} depicted in Fig. 1, the plant $P(s)$ is assumed to be a second order time delay model whose standard form is expressed as

$$P(s) = \frac{\omega^2 e^{-Ls}}{s^2 + 2\zeta\omega s + \omega^2} \quad (3)$$

The natural frequency ω, damping rate ζ, and time delay L are the specified characteristic parameters. Because of the typical dual-circuit structure, a cascade control strategy regulates two cascaded processes that are split by a controlled process $P(s)$. One process $P_2(s)$ with a smaller time-constant and stronger disturbance is suitable to be placed into the secondary loop. The other process $P_1(s)$ that is put into the primary loop possesses a larger time constant and time delay. The decomposition from a SOPTD plant to two first order plus time delay plants (FOPTD) makes use of the Fundamental theorem of algebra. Given a second-order system with time-delay expressed by (3), it can be rewritten as

$$P(s) = P_2(s)P_1(s) = \frac{K_2 e^{-L_2 s}}{aTs + 1} \frac{K_1 e^{-L_1 s}}{Ts + 1} \quad (4)$$

where K_1, L_1, and T are the gain, time delay, and time constant of the plant $P_1(s)$. In addition, K_2 and L_2 are the gain and time delay of the plant $P_2(s)$. As pointed out before, the time constant is expected to be as small as possible for the controlled plant $P_2(s)$ of the secondary loop. Therefore, the time constant ratio of $P_2(s)$ and $P_1(s)$ is set to satisfy $0 \leq a \leq 1$.

Remark 1: To correspond with the double loop structure of the control system Σ_{CCS}, this part divides the second-order time-delay process $P(s)$ into two first-order time-delay processes, the primary and the secondary plant. Meanwhile, the decomposition strategy settles the problem that the SOPTD model has a higher order that hinders the design of CRNs. Therefore, the division of second-order time delay plants also provides the possibility for the realization of CRNs in the future, except for the needs of the cascade control system's structure. More details are presented in Section III.

The design of the cascade PID controller $C_{CCS}(s)$, which is composed of the primary controller $C_1(s)$ and the secondary
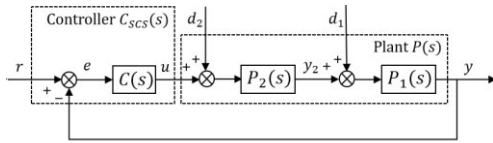
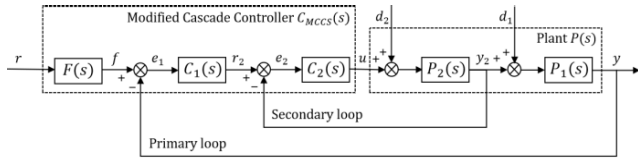**FIGURE 2.** Structure of single-loop control system Σ_{SCS}.

FIGURE 3. Structure of modified cascade control system Σ_{MCCS}.

controller $C_2(s)$, is based on the model of the controlled process described above. The secondary disturbance d_2 occurring in the secondary process is assigned to the inner loop, which enables it to be rejected by the secondary controller $C_2(s)$ in time. Furthermore, the secondary loop's output signal y_2 acting as the manipulated variable does not need to be precisely controlled. Hence a PI controller is chosen as the secondary controller of the cascade control system, and its transfer function is

$$C_2(s) = k_{P2} + k_{I2}\frac{1}{s} \tag{5}$$

where k_{P2} is the proportional gain, and k_{I2} is the integral gain. To avoid tedious trials and errors, the parameters of the controller $C_2(s)$ are obtained by means of analysis [19]. The reference model, which is depicted by (6), defines the required closed-loop behavior of the secondary loop.

$$M_2(s) = \frac{e^{-L_2 s}}{T_2 s + 1} \tag{6}$$

where T_2 is the time constant of the $M_2(s)$ and L_2 is the time delay of $P_2(s)$. With the reference model $M_2(s)$ represented by (6) and the transfer function $F_{y_2 r_2}(s)$ shown in (1), the controller $C_2(s)$ based on the plant $P_2(s)$ is given by

$$C_2(s) = \frac{aTs + 1}{K_2(T_2 s + 1 - e^{-L_2 s})} \tag{7}$$

Utilizing the Maclaurin series, the ideal controller indicated by (7) approximates to a PI controller indicated by (5). As a result, k_{P2} and k_{I2} in (5) are determined by

$$k_{P2} = \frac{1}{K_2(T_2 + L_2)}\left(aT + \frac{L_2^2}{2(T_2 + L_2)}\right) \tag{8}$$

and

$$k_{I2} = \frac{1}{K_2(T_2 + L_2)} \tag{9}$$

Since the primary loop must try its best to control the controlled variable y accurately, the PID controller is considered to serve as the primary controller $C_1(s)$, whose transfer

function is provided by

$$C_1(s) = k_{P1} + k_{I1}\frac{1}{s} + k_{D1}s \tag{10}$$

where k_{P1}, k_{I1}, and k_{D1} are tuning parameters, corresponding in turn to proportional, integral, and derivative gains. Similar to the secondary loop, the reference model for the primary loop is obtained by

$$M_1(s) = \frac{e^{-(L_1+L_2)s}}{T_1 s + 1} \tag{11}$$

where T_1 is closely associated with the expected primary loop response. Additionally, L_1 and L_2 are the time delays of the controlled processes $P_1(s)$ and $P_2(s)$. A controlled plant consisting of the reference model $M_2(s)$ in the inner loop and the primary plant $P_1(s)$ in the outer loop is shown in

$$P_3(s) = \frac{K_1 e^{-(L_1+L_2)s}}{(Ts+1)(T_2 s+1)} \tag{12}$$

Based on the plant $P_3(s)$, the ideal primary controller is derived from

$$C_1(s) = \frac{(Ts+1)(T_2 s+1)}{K_1 e^{-L_2 s}(T_1 s+1-e^{-(L_1+L_2)s})} \tag{13}$$

The controller is equivalently transformed into a PID controller, shown in (10), by using the Maclaurin series. The tuning parameters k_{P1}, k_{I1}, and k_{D1} are set as follows:

$$k_{P1} = \frac{1}{K_1(T_1+L_1+L_2)}\left(T+T_2+\frac{(L_1+L_2)^2}{2(T_1+L_1+L_2)}\right) \tag{14}$$

$$k_{I1} = \frac{1}{K_1(T_1+L_1+L_2)} \tag{15}$$

and

$$k_{D1} = k_{P1}\left\{\frac{T_2 T - \frac{(L_1+L_2)^3}{6(T_1+L_1+L_2)}}{T+T_2+\frac{(L_1+L_2)^2}{2(T_1+L_1+L_2)}} + \frac{(L_1+L_2)^2}{2(T_1+L_1+L_2)}\right\} \tag{16}$$

Remark 2: Different from the cascade control system Σ_{CCS}, the single-loop control system (SCS) Σ_{SCS} stated by Fig. 2 has no more than a feedback loop. The feedback prevents the state of the controlled process from being fed back and adjusted timely, which destroys the stability of the system Σ_{SCS}. It can be found from Fig. 2 that the controlled variable y is inevitably affected if the manipulated variable y_2 of the controlled plant $P(s)$ encounters secondary disturbance d_2. In fact, internal perturbations d_2 are widespread in biochemical systems, such as overexpression of the IRF4 and IRF5 genes in the polarization process of TAMs. In the following, in order to quickly eliminate the effects of gene overexpression and endogenous genes on gene expression, a modified cascade PID control method is applied to control both the transcription and translation of the IRF4 and IRF5 genes. In contrast, the single-loop PID control method can regulate the IRF4 and IRF5 genes at either the transcriptional

TABLE 1. Parameters of the modified cascade control system Σ_{MCCS}.

Module	Parameter
First-order low-pass filter $F(s)$	$T_f = 250$
Primary controller $C_1(s)$	$k_{P1} = 2.291$ $k_{I1} = 0.0035$ $k_{D1} = 253.575$
Secondary controller $C_2(s)$	$k_{P2} = 3.336$ $k_{I2} = 0.007$
Primary process $P_1(s)$	$K_1 = 1$ $T = 500$ $L_1 = 20$
Secondary process $P_2(s)$	$K_2 = 1$ $aT = 500$ $L_2 = 10$

TABLE 2. The comparison of control system Σ_{CCS} without filter coefficients T_f and control system Σ_{MCCS} with five different filter coefficients T_f.

Control system	Filter coefficient T_f	Maximum control signal u_{max}	Overshoot δ_O (%)	Settling time t_s (s)
Σ_{CCS} [19]	-	7.85	3.646	1623
Σ_{MCCS}	125	7.06	0	1345
	150	5.947	0	1365
	200	4.579	0	1464
	250	3.712	0	1596
	300	3.121	0	1746

FIGURE 4. The control signal u in the modified cascade control system Σ_{MCCS} and the cascade control system Σ_{CCS} responding to a reference signal $r = 1$.

FIGURE 5. The responses y of the control systems Σ_{MCCS} and Σ_{CCS} correspond to the control signal u in FIGURE. 4.

or translational levels. A single-loop PID control strategy to control the translation process is recommended in this paper to ensure that the genes IRF4 and IRF5 are exactly expressed.
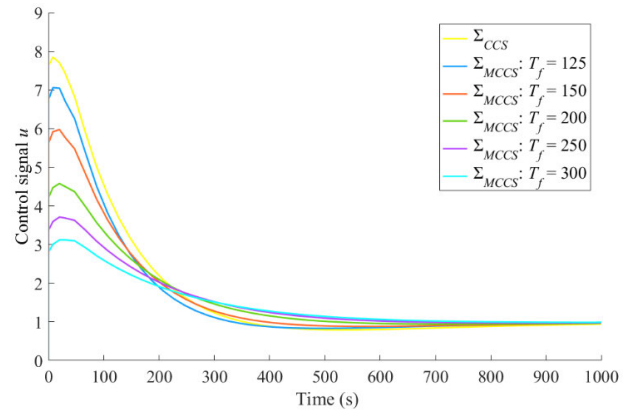
B. IMPROVEMENT OF CASCADE PID CONTROL SYSTEMS

The previous part designed a cascade PID control system Σ_{CCS}, where the primary controller $C_1(s)$ works in coordination with the secondary controller $C_2(s)$. Nevertheless, the two cascaded controllers continuously amplify the control signal u input to the controlled object $P(s)$ while the reference signal r is initialized. Consequently, the system overshoot is easily generated, and the DNA species are largely wasted. For this reason, the first-order low-pass filter $F(s)$ is introduced to modify the cascade PID controller C_{CCS} [19].
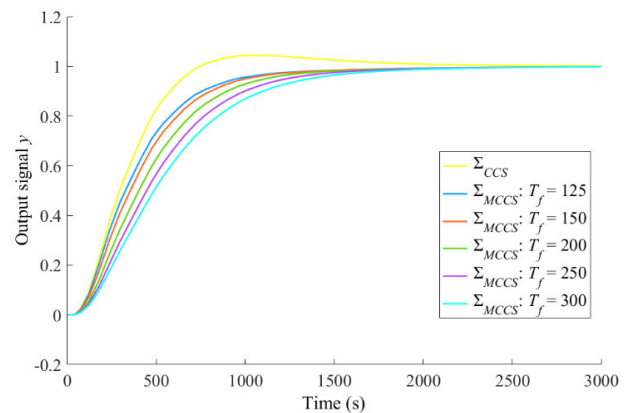
The modified cascade control system Σ_{MCCS} is described by Fig. 3. In the presented control system, the reference input signal r is first processed by a first-order low-pass filter $F(s)$, whose standard form is expressed by

$$F(s) = \frac{1}{T_f s + 1} \qquad (17)$$

where T_f is the filter coefficient that is associated with the filter's corner frequency $f_c = 1/(2\pi T_f)$. By filtering

out frequencies of the reference input above the corner frequency, the filter alters the cascade controller's output signal in response to the reference signal. To further investigate how the control signal u is affected, the filter coefficient is assumed to be different values. Also, the cascade PID control system Σ_{CCS} proposed in [19] is used for comparison.

Example 1: Examine the modified cascade PID control system Σ_{MCCS}, using the parameters illustrated in Table 1. Since the controller is obtained according to the controlled plants and reference models, the design strategies of the controllers $C_1(s)$ and $C_2(s)$ in the modified cascade PID controller $C_{MCCS}(s)$ and the cascade PID controller $C_{CCS}(s)$ are consistent.

The response curves of the control signal u for the control strategies Σ_{MCCS} and Σ_{CCS} are plotted in Fig. 4 under the condition of the reference signal $r = 1$. In particular, $T_f = \{125, 150, 200, 250, 300$ is taken into account in the improved cascade PID control system. It is apparent in Fig. 4 that the control signal of the control system Σ_{MCCS} diminishes significantly as the filter coefficient decreases. As illustrated in Table 2, when the filter coefficient T_f is 250,

the maximum control signal u_{max} output by the controller $C_{MCCS}(s)$ is 3.712, which is 47.28% of the maximum control signal generated by the controller $C_{CCS}(s)$. There is no doubt that the filter $F(s)$ regulating the dynamic of the reference signal reduces the consumption of energy caused by the excess of the control signal.

The plant $P(s)$ takes the control signal u in Fig. 4 as input and produces the output y in Fig. 5. Obviously, given the reference signal, the control system Σ_{MCCS} has no overshoot but the control system Σ_{CCS} has an overshoot of 3.646%. Furthermore, the output generated by the improved cascade control system slows down the tracking of the input r with the decrease of the filter coefficient T_f. Given the above, although the increase in the filter coefficient means a reduction in the speed of the tracking reference signal, the introduction of the filter significantly diminishes the control signal and overshoot. In fact, the modified cascade control system reaches a steady state faster than the cascade control system because of overshoot's elimination.

Remark 3: To reduce the waste of the DNA species and the overshoot of the control systems caused by the oversized control signal, a first-order low-pass filter is integrated into the cascade PID control system in this part. The filter $F(s)$ is researched on the impact of the control signal u by assigning different values to the filter coefficients T_f. When the controller $C_{MCCS}(s)$ controls the plant $P(s)$ to track a set point, the maximum control signal u_{max} becomes smaller by decreasing T_f, as stated in Table 2. Meanwhile, output curves of the improved cascade control system depicted by Fig. 5 no longer exist the overshoot. In order to maintain that control system Σ_{MCCS} has a faster output response y than control system Σ_{CCS}, while the control signal is decreased, the parameter of the filter $F(s)$ in Table 1 is finally determined to be 250.

III. CASCADE PID CONTROL SYSTEM BASED ON CRNS

By coupling with a first-order low-pass filter, the cascade control system is improved. Afterward, the CRNs of the modified control system are designed and simulated in this section. First, the cascade PID control strategy is implemented by employing CRNs to control a second-order time-delay process $P(s)$. Next, the effectiveness and superiority of the CRNs-based cascade PID control method are verified by comparison with the CRN-based single-loop PID control method. The simulation of the system Σ_{MCCS} and Σ_{SCS} considers the ability to track the reference input r, reject the primary disturbance d_1, suppress the secondary disturbance d_2, and attenuate both the disturbance d_1 and d_2.

A. CRNS DESIGN OF SECOND-ORDER PROCESSES WITH TIME DELAY

The controlled plant in the cascade PID control system Σ_{MCCS} is a second-order time delay system represented by (3). The design of the CRNs for the system $P(s)$ is a tricky problem owing to the high order and nonlinear time-delay. As described in (4), a second-order time-delay process can be decomposed into two first-order time delay processes, which
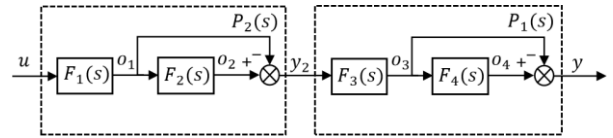
FIGURE 6. The controlled plant $P(s)$ of the cascade PID control system, a second-order time-delay system, is decomposed into four first-order systems $F_1(s)$, $F_2(s)$, $F_3(s)$, and $F_4(s)$.

act as the primary plant $P_1(s)$ and the secondary plant $P_2(s)$ in the control system Σ_{MCCS}. Then the time-delay terms for the plants $P_1(s)$ and $P_2(s)$ are re-expressed by the first-order Padé approximation, that is, $e^{-L_1 s} = (2 - L_1 s)/(2 + L_1 s)$ and $e^{-L_2 s} = (2 - L_2 s)/(2 + L_2 s)$. As a result, the primary and secondary plants in (4) are rewritten as
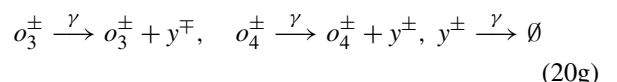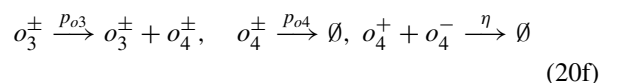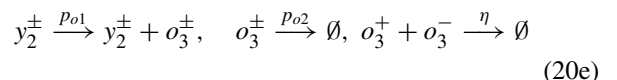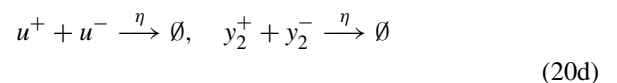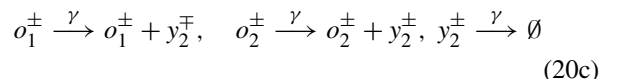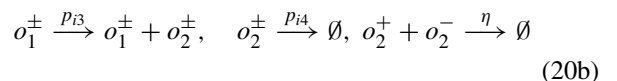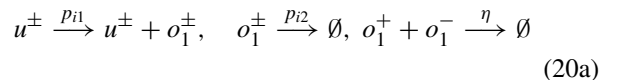
$$P_1(s) = F_3(s)(F_4(s) - 1) = \frac{p_{o1}}{s + p_{o2}}\left(\frac{p_{o3}}{s + p_{o4}} - 1\right) \quad (18)$$

and

$$P_2(s) = F_1(s)(F_2(s) - 1) = \frac{p_{i1}}{s + p_{i2}}\left(\frac{p_{i3}}{s + p_{i4}} - 1\right) \quad (19)$$

In (18), $p_{o1} = K_1/T$, $p_{o2} = 1/T$, $p_{o3} = 4/L_1$, and $p_{o4} = 2/L_1$. And in (19), $p_{i1} = K_2/aT$, $p_{i2} = 1/aT$, $p_{i3} = 4/L_2$, and $p_{i4} = 2/L_2$. As shown in Fig. 6, a second-order time delay system is divided into four first-order systems (i.e., $F_1(s)$, $F_2(s)$, $F_3(s)$, and $F_4(s)$), introducing five state variables (i.e., o_1, o_2, o_3, o_4, and y_2).

Applying the dual-rail representation, each signal in Fig. 6 is assigned a pair of chemical species to obtain the CRNs of a second-order process with time-delay.

$$u^{\pm} \xrightarrow{p_{i1}} u^{\pm} + o_1^{\pm}, \quad o_1^{\pm} \xrightarrow{p_{i2}} \emptyset, \quad o_1^+ + o_1^- \xrightarrow{\eta} \emptyset \quad (20a)$$

$$o_1^{\pm} \xrightarrow{p_{i3}} o_1^{\pm} + o_2^{\pm}, \quad o_2^{\pm} \xrightarrow{p_{i4}} \emptyset, \quad o_2^+ + o_2^- \xrightarrow{\eta} \emptyset \quad (20b)$$

$$o_1^{\pm} \xrightarrow{\gamma} o_1^{\pm} + y_2^{\mp}, \quad o_2^{\pm} \xrightarrow{\gamma} o_2^{\pm} + y_2^{\pm}, \quad y_2^{\pm} \xrightarrow{\gamma} \emptyset \quad (20c)$$

$$u^+ + u^- \xrightarrow{\eta} \emptyset, \quad y_2^+ + y_2^- \xrightarrow{\eta} \emptyset \quad (20d)$$

$$y_2^{\pm} \xrightarrow{p_{o1}} y_2^{\pm} + o_3^{\pm}, \quad o_3^{\pm} \xrightarrow{p_{o2}} \emptyset, \quad o_3^+ + o_3^- \xrightarrow{\eta} \emptyset \quad (20e)$$

$$o_3^{\pm} \xrightarrow{p_{o3}} o_3^{\pm} + o_4^{\pm}, \quad o_4^{\pm} \xrightarrow{p_{o4}} \emptyset, \quad o_4^+ + o_4^- \xrightarrow{\eta} \emptyset \quad (20f)$$

$$o_3^{\pm} \xrightarrow{\gamma} o_3^{\pm} + y^{\mp}, \quad o_4^{\pm} \xrightarrow{\gamma} o_4^{\pm} + y^{\pm}, \quad y^{\pm} \xrightarrow{\gamma} \emptyset \quad (20g)$$

$$y^+ + y^- \xrightarrow{\eta} \emptyset \quad (20h)$$

Equations (20a)-(20d) represent the CRNs of the secondary process, and (20e)-(20h) realize the CRNs of the primary process. In the plants $P_1(s)$ and $P_2(s)$, the time delays
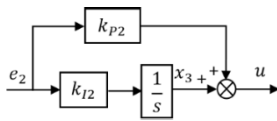
FIGURE 7. The block diagram of the secondary controller $C_2(s)$ for the CRNs implementation.
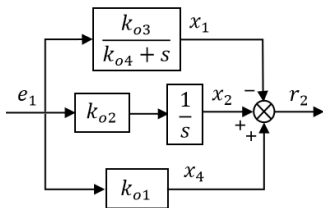

FIGURE 8. The structure of the approximated primary controller $C_1(s)$ for the CRNs representation [10].
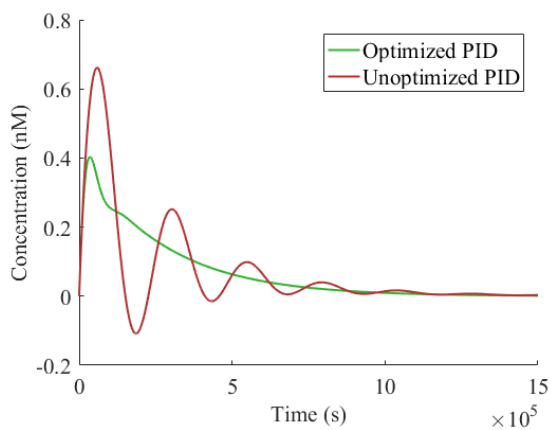

FIGURE 9. The error e_1 of the optimized CRNs-based PID controller and the unoptimized CRNs-based PID controller.

L_1 and L_2 are approximated by equations (20b)-(20d) and (20f)-(20h), respectively.

Using the law of mass action, each signal dynamic in the CRNs constructing the second-order time delay plant is derived from the ordinary differential equation, as follows:

$$\dot{o}_1^\pm = p_{i1}u^\pm - p_{i2}o_1^\pm - \eta o_1^+ o_1^- \tag{21a}$$

$$\dot{o}_2^\pm = p_{i3}o_1^\pm - p_{i4}o_2^\pm - \eta o_2^+ o_2^- \tag{21b}$$

$$\dot{y}_2^\pm = \gamma o_1^\mp + \gamma o_2^\pm - \gamma y_2^\pm - \eta y_2^+ y_2^- \tag{21c}$$

$$\dot{o}_3^\pm = p_{o1}y_2^\pm - p_{o2}o_3^\pm - \eta o_3^+ o_3^- \tag{21d}$$

$$\dot{o}_4^\pm = p_{o3}o_3^\pm - p_{o4}o_4^\pm - \eta o_4^+ o_4^- \tag{21e}$$

$$\dot{y}^\pm = \gamma o_3^\mp + \gamma o_4^\pm - \gamma y^\pm - \eta y^+ y^- \tag{21f}$$

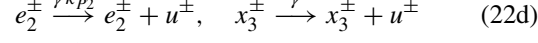## B. CRNS REALIZATION OF CASCADE PID CONTROL STRATEGIES FOR SECOND-ORDER TIME DELAY PROCESSES
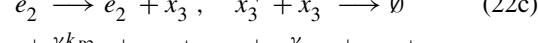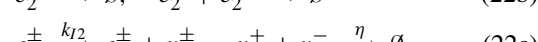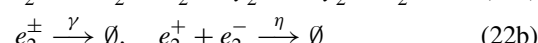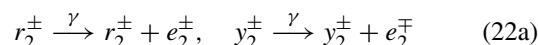
As the controlled plant of the cascade PID control system Σ_{MCCS}, the second-order time delay plant is built by utilizing the CRNs ((20a)-(20h)). Subsequently, the CRNs design for

TABLE 3. DSD reactions and DNA species required to implement DSD networks for optimized and unoptimized CRN-based PID controllers.

PID controller	DSD reactions	DNA species
Unoptimized CRN [10]	63	87
Optimized CRN	51	71

the control system Σ_{MCCS} is supplemented in the section, which includes the representation of the CRNs for the first-order low-pass filter, the primary controller and the secondary controller.

In the cascade PID control system, the inner loop contains the secondary controller illustrated by (5), apart from the secondary process. A PI controller shown in Fig. 7 is chosen as the secondary controller $C_2(s)$, whose CRNs are as follows:

$$r_2^\pm \xrightarrow{\gamma} r_2^\pm + e_2^\pm, \quad y_2^\pm \xrightarrow{\gamma} y_2^\pm + e_2^\mp \tag{22a}$$

$$e_2^\pm \xrightarrow{\gamma} \emptyset, \quad e_2^+ + e_2^- \xrightarrow{\eta} \emptyset \tag{22b}$$

$$e_2^\pm \xrightarrow{k_{I2}} e_2^\pm + x_3^\pm, \quad x_3^+ + x_3^- \xrightarrow{\eta} \emptyset \tag{22c}$$

$$e_2^\pm \xrightarrow{\gamma k_{P2}} e_2^\pm + u^\pm, \quad x_3^\pm \xrightarrow{\gamma} x_3^\pm + u^\pm \tag{22d}$$

$$u^\pm \xrightarrow{\gamma} \emptyset, \quad u^+ + u^- \xrightarrow{\eta} \emptyset \tag{22e}$$

The error signal e_2 that is input to the secondary controller is generated by (22a)-(22b). Especially, the specie y^+ has a negative effect on the specie e^+, which is expressed by the inversion of the superscript. The weighted integral module $k_{I2}(1/s)$ is precisely realized by (22c) in the PI controller constructed by (22c)-(22e). The summation of the weighted error signal $k_{P2}e_2$ and the unweighted signal x_2 is calculated by (22d)-(22e).

As a part of the primary loop, the CRNs of a complete secondary loop is built by (20a)-(20d) and (22a)-(22e). In addition, the primary loop also comprises the primary controller and the first-order low-pass filter, whose transfer functions are defined by (10) and (17). For the purpose of designing CRNs, this first-order low-pass filter is rewritten as

$$F(s) = \frac{k_f}{s + k_f} \tag{23}$$

where $k_f = 1/T_f$. As described in (10), the primary controller selects the PID controller, where the differential is required to be linearized by the Padé approximation. Thus, the primary controller is re-expressed by Fig. 8 and (24).

$$C_1(s) = k_{o1} + k_{o2}\frac{1}{s} - \frac{k_{o3}}{k_{o4} + s} \tag{24}$$

In (24), $k_{o1} = k_{P1} + 2k_{D1}/\tau$, $k_{o2} = k_{I1}$, $k_{o3} = 4k_{D1}/\tau^2$, and $k_{o4} = 2/\tau$.

Each signal in Fig. 8 (i.e., e_1, x_1, x_2, x_4, and r_2) is represented by a pair of chemical species. In order to generate a
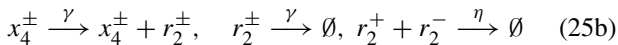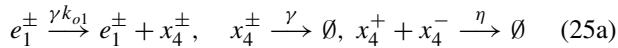
TABLE 4. Parameters of the CRNs-based control systems Σ_{MCCS} and Σ_{SCS} in Example 2.

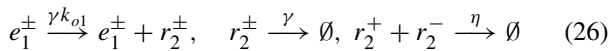| Control system Σ_{MCCS}	Control system Σ_{SCS}
$C_{MCCS}(s)\begin{cases} F(s)\{k_f = 0.004 \\ C_1(s)\begin{cases} k_{o1} = 12.434 \\ k_{o2} = 0.0035 \\ k_{o3} = 0.406 \\ k_{o4} = 0.04 \end{cases} \\ C_2(s)\begin{cases} k_{P1} = 3.336 \\ k_{I1} = 0.007 \end{cases} \end{cases}$	$C_{SCS}(s)\begin{cases} k_1 = 39.517 \\ k_2 = 0.004 \\ k_3 = 1.438 \\ k_4 = 0.04 \end{cases}$
$P(s)\begin{cases} P_2(s)\begin{cases} p_{i1} = 0.002 \\ p_{i2} = 0.002 \\ p_{i3} = 0.4 \\ p_{i4} = 0.2 \end{cases} \\ P_2(s)\begin{cases} p_{o1} = 0.002 \\ p_{o2} = 0.002 \\ p_{o3} = 0.2 \\ p_{o4} = 0.1 \end{cases} \end{cases}$	$P(s)\begin{cases} P_2(s)\begin{cases} p_{i1} = 0.002 \\ p_{i2} = 0.002 \\ p_{i3} = 0.4 \\ p_{i4} = 0.2 \end{cases} \\ P_2(s)\begin{cases} p_{o1} = 0.002 \\ p_{o2} = 0.002 \\ p_{o3} = 0.2 \\ p_{o4} = 0.1 \end{cases} \end{cases}$

FIGURE 10. The output trajectories of control systems Σ_{MCCS} and Σ_{SCS} based on CRNs for step changes.

TABLE 5. Overshoot of CRNs-based control systems Σ_{MCCS} and Σ_{SCS} in response to step changes.

Control system	Overshoot δ_1	Overshoot δ_2	Overshoot δ_3
Σ_{SCS} [10]	1.016%	2.032%	3.048%
Σ_{MCCS}	0.4%	0.801%	0.012%

FIGURE 11. Under the condition of the reference input signal $r = 0$, the output responses of the CRNs-based control systems Σ_{MCCS} and Σ_{SCS} to the secondary disturbance $d_2 = 1$.

summation signal r_2, signal x_4 must first be output by signal e_1 through a proportional block, as shown in (25).

$$e_1^{\pm} \xrightarrow{\gamma k_{o1}} e_1^{\pm} + x_4^{\pm}, \quad x_4^{\pm} \xrightarrow{\gamma} \varnothing, \; x_4^+ + x_4^- \xrightarrow{\eta} \varnothing \quad (25a)$$

$$x_4^{\pm} \xrightarrow{\gamma} x_4^{\pm} + r_2^{\pm}, \quad r_2^{\pm} \xrightarrow{\gamma} \varnothing, \; r_2^+ + r_2^- \xrightarrow{\eta} \varnothing \quad (25b)$$
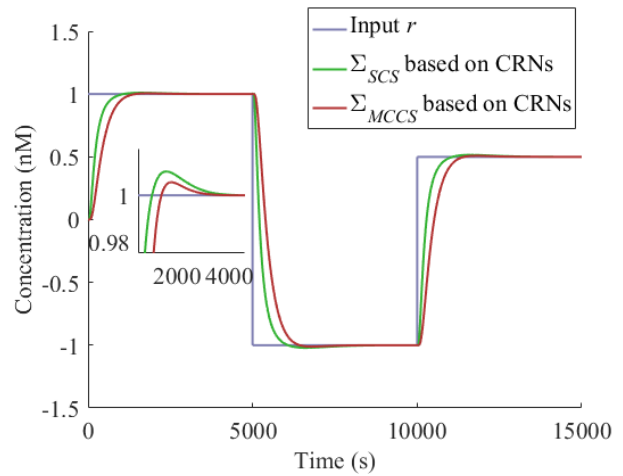
However, this is not necessary. An optimization method named weighted summation is presented in this paper to reduce the chemical species and reactions required to realize PID controllers. In the proposed method, signal e_1 can directly produce signal r_2, as described in (26).
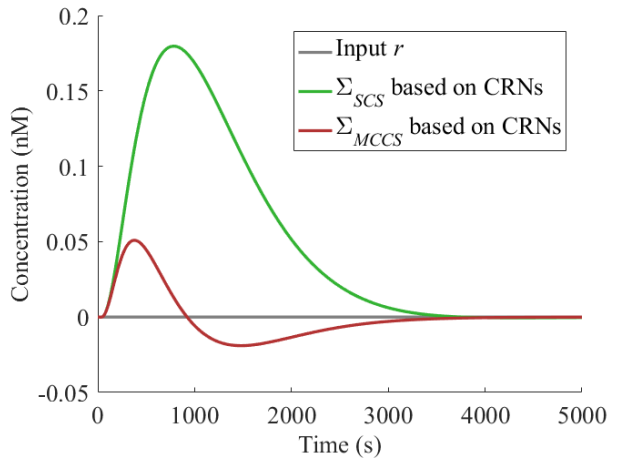
$$e_1^{\pm} \xrightarrow{\gamma k_{o1}} e_1^{\pm} + r_2^{\pm}, \quad r_2^{\pm} \xrightarrow{\gamma} \varnothing, \; r_2^+ + r_2^- \xrightarrow{\eta} \varnothing \quad (26)$$

The ordinary differential equation of (26) is as follows:

$$\dot{r}_2^{\pm} = \gamma k_{o1} e_1^{\pm} - \gamma r_2^{\pm} - \eta r_2^+ r_2^- \quad (27)$$

If the CRN denoted by (26) reaches the steady state, then $r_2 = k_{o1} e_1$. Meanwhile, the signal r_2 is also catalytically generated by other weighted or unweighted signals. The summation of the signal e_1 with other signals is achieved by accumulating the concentration of the chemical species $r_2^{\pm}$ due to the same degradation rate. As shown in Fig. 9, the optimized PID more quickly and stably obtains a zero steady-state error, since the gain block no longer requires a separate approximation implementation. Furthermore, the optimized CRN-based PID controller requires fewer chemical reactions
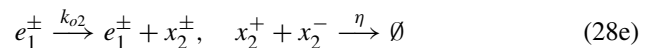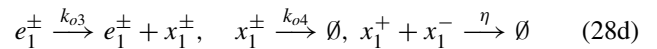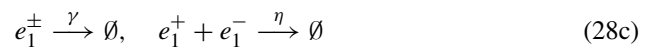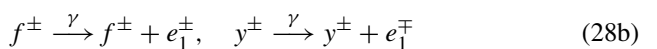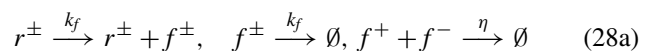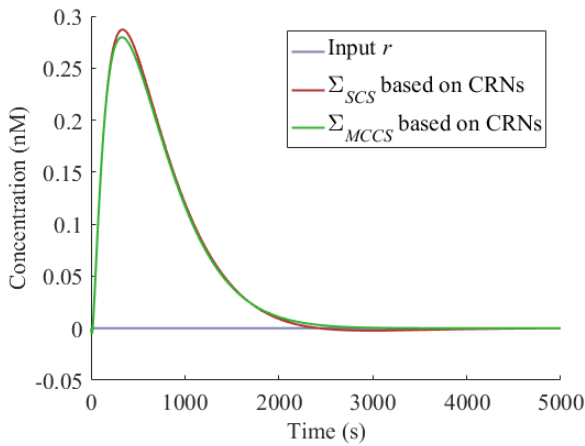
and species, resulting in a corresponding DSD reaction network with fewer DSD reactions and DNA species. When DSD reactions are adopted to implement PID controllers, as illustrated in Table 3, the unoptimized CRNs require 63 reactions and 87 chains, whereas the optimized CRNs only need 51 reactions and 71 chains.

Based on the above discussions, the filter $F(s)$ and the controller $C_2(s)$ are established by the following CRNs.

$$r^{\pm} \xrightarrow{k_f} r^{\pm} + f^{\pm}, \quad f^{\pm} \xrightarrow{k_f} \varnothing, \; f^+ + f^- \xrightarrow{\eta} \varnothing \quad (28a)$$

$$f^{\pm} \xrightarrow{\gamma} f^{\pm} + e_1^{\pm}, \quad y^{\pm} \xrightarrow{\gamma} y^{\pm} + e_1^{\mp} \quad (28b)$$

$$e_1^{\pm} \xrightarrow{\gamma} \varnothing, \quad e_1^+ + e_1^- \xrightarrow{\eta} \varnothing \quad (28c)$$

$$e_1^{\pm} \xrightarrow{k_{o3}} e_1^{\pm} + x_1^{\pm}, \quad x_1^{\pm} \xrightarrow{k_{o4}} \varnothing, \; x_1^+ + x_1^- \xrightarrow{\eta} \varnothing \quad (28d)$$

$$e_1^{\pm} \xrightarrow{k_{o2}} e_1^{\pm} + x_2^{\pm}, \quad x_2^+ + x_2^- \xrightarrow{\eta} \varnothing \quad (28e)$$

FIGURE 12. The closed-loop responses of the CRNs-based control systems Σ_{MCCS} and Σ_{SCS}, when the reference input signal and primary disturbance are $r = 0$ and $d_1 = 1$ respectively.
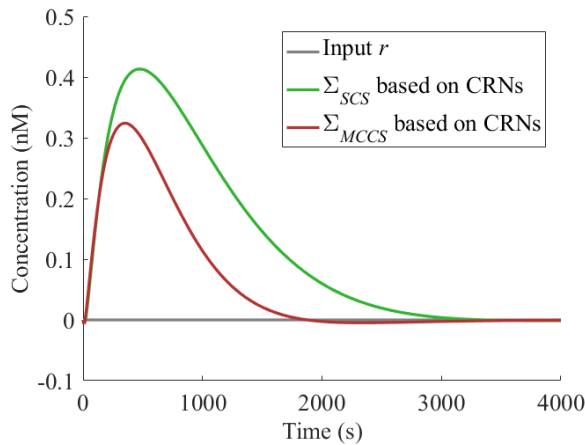
FIGURE 13. For the primary disturbance $d_1 = 1$ and the secondary disturbance $d_2 = 1$, the responses of the CRNs-based control systems Σ_{MCCS} and Σ_{SCS} to the reference signal $r = 0$.

$$e_1^{\pm} \xrightarrow{\gamma k_{o1}} e_1^{\pm} + r_2^{\pm}, \quad x_1^{\pm} \xrightarrow{\gamma} x_1^{\pm} + r_2^{\mp}, \quad x_2^{\pm} \xrightarrow{\gamma} x_2^{\pm} + r_2^{\pm}$$ (28f)

$$r_2^{\pm} \xrightarrow{\gamma} \emptyset, \quad r_2^{+} + r_2^{-} \xrightarrow{\eta} \emptyset$$ (28g)

In the above CRNs, (28a) and (28b)-(28g) respectively realize the first-order low-pass filter and the primary controller. The error signal e_1 of the outer loop is obtained from (28b)-(28c), where the negative feedback is achieved in (28b) via the cross contribution of $y^{\pm}$ to $e_1^{\mp}$. The first-order system $k_{o3}/(k_{o4} + s)$ and the weighted integral $k_{o2}(1/s)$ in the approximated primary controller are accurately expressed by (28d) and (28e). A cascade PID control system at the steady state allows (28f)-(28g) to approximate the summation results of $k_{o1}e_1$, x_1, and x_2.

Based on the mass action law, the following equations represent the kinetics of the signal in the CRNs of (22a)-(22e)

TABLE 6. Parameters of the DSD-based controllers $C_{MCCS}(s)$ and $C_{SCS}(s)$ in Example 3.

Controller $C_{MCCS}(s)$		Controller $C_{SCS}(s)$	
$F(s)\{q_f = 0.0125$			
$C_1(s)$	$\begin{cases} q_{o1} = 12.434 \\ q_{o2} = 0.00875 \\ q_{o3} = 1.015 \\ q_{o4} = 0.1 \end{cases}$	$C(s)$	$\begin{cases} q_1 = 39.517 \\ q_2 = 0.067 \\ q_3 = 23.967 \\ q_4 = 0.667 \end{cases}$
$C_2(s)$	$\begin{cases} q_{i1} = 3.336 \\ q_{i2} = 0.0175 \end{cases}$		

TABLE 7. Overshoot of control systems Σ_{MCCS} and Σ_{SCS} Based on DSD in response to the disturbances.

Disturbance input	Overshoot δ_o (%) of Σ_{SCS} [10]	Overshoot δ_o (%) of Σ_{MCCS}
$d_1 = 0, d_2 = 10^{-6}$	16.79	0
$d_1 = 10^{-6}, d_2 = 0$	32.966	6.982
$d_1 = 10^{-6}, d_2 = 10^{-6}$	33.988	6.281

and (28a)-(28g):

$$\dot{f}^{\pm} = k_f r^{\pm} - k_f f^{\pm} - \eta f^{+} f^{-}$$ (29a)

$$\dot{e}_1^{\pm} = \gamma f^{\pm} + \gamma y^{\mp} - \gamma e_1^{\pm} - \eta e_1^{+} e_1^{-}$$ (29b)

$$\dot{x}_1^{\pm} = k_{o3} e_1^{\pm} - k_{o4} x_1^{\pm} - \eta x_1^{+} x_1^{-}$$ (29c)

$$\dot{x}_2^{\pm} = k_{o2} e_1^{\pm} - \eta x_2^{+} x_2^{-}$$ (29d)

$$\dot{r}_2^{\pm} = \gamma k_{o1} e_1^{\pm} + \gamma x_1^{\pm} + \gamma x_2^{\pm} - \gamma r_2^{\pm} - \eta r_2^{+} r_2^{-}$$ (29e)

$$\dot{e}_2^{\pm} = \gamma r_2^{\pm} + \gamma y_2^{\mp} - \gamma e_2^{\pm} - \eta e_2^{+} e_2^{-}$$ (29f)

$$\dot{x}_3^{\pm} = k_{I2} e_2^{\pm} - \eta x_3^{+} x_3^{-}$$ (29g)

$$\dot{u}^{\pm} = \gamma k_{P2} e_2^{\pm} + \gamma x_3^{\pm} - \gamma u^{\pm} - \eta u^{+} u^{-}$$ (29h)

C. THE VALIDITY OF CASCADE PID CONTROL SYSTEMS BASED ON CRNS

The effectiveness of the cascade PID control strategy based on CRNs is verified in this part by a simulation. The control effects of control systems Σ_{MCCS} and Σ_{SCS} are considered for the following four input cases: the first is the tracking of step changes, the second is the rejection of secondary disturbances, the third is the suppression of primary disturbances, and the fourth is the attenuation of both the primary and secondary disturbances.

Example 2: The CRNs-based cascade PID control system Σ_{MCCS} (Fig. 3) is compared with the CRNs-based single-loop PID control system Σ_{SCS} [10] (Fig. 2). Table 4 provides a description of all parameters.

When the step changes exist in the given reference signal, the closed-loop response of the cascade PID control strategy and the single-loop PID control strategy varies with time in Fig. 10. The fact is that the response y of two control systems ultimately results in a zero steady-state error for following
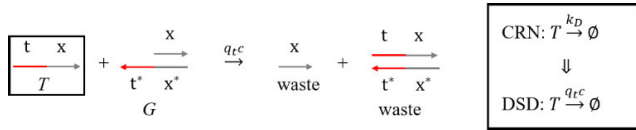
FIGURE 14. DSD implementation of the degradation reaction, where $q_tc = k_D C_{max}^{-1}$ [33].
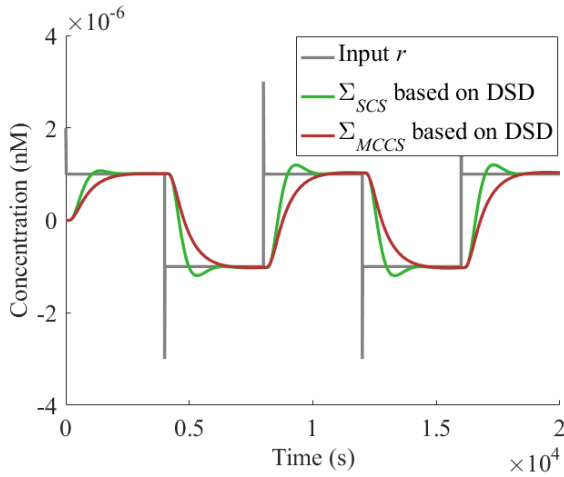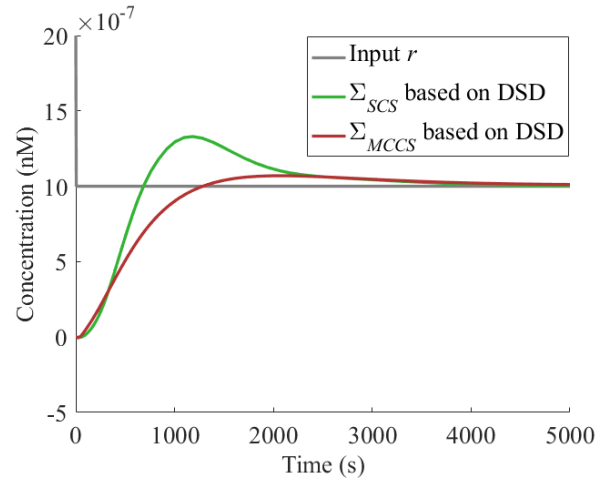

FIGURE 15. The output trajectories of the control systems Σ_{MCCS} and Σ_{SCS} based on DSD reactions when the reference input signal with step changes is given.
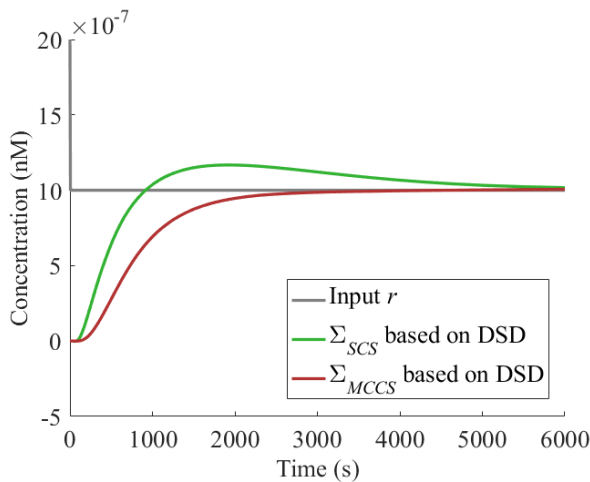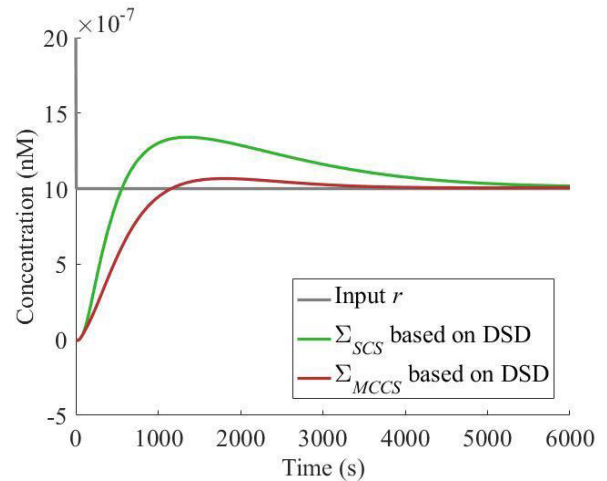

FIGURE 16. The output responses of the DSD-based control systems Σ_{MCCS} and Σ_{SCS} while a secondary disturbance is fed into the secondary plant.

FIGURE 17. The set-point responses of the DSD-based control systems Σ_{MCCS} and Σ_{SCS} to the primary disturbance.

FIGURE 18. The closed-loop responses of the DSD-based control systems Σ_{MCCS} and Σ_{SCS} for tracking the reference signal, assuming that the primary and secondary disturbances perturb the operation of the control system at the same time.

the reference signal. However, the system Σ_{MCCS} exhibits a smoother response than the system Σ_{SCS}, which can be observed from the overshoot described in Table 5. δ_1, δ_2, and δ_3 in Table 5 represent the overshoot of the control systems for tracking step signals $r = 1$, $r = -1$, and $r = 0.5$, respectively. The above results indicate that the cascade PID control strategy based on CRNs can meet the pursuit of control performance indicators with higher-level precision.

Given the secondary disturbance $d_2 = 1$ and reference input $r = 0$, Fig. 11 displays the output curves for the control systems Σ_{MCCS} and Σ_{SCS} that are constructed by employing the CRNs. The cascade PID controller outperforms the single-loop PID controller with a slight influence of secondary disturbance on the output y of the controlled process. As previously stated, the secondary disturbance in the inner loop is suppressed timely by the secondary controller. It is indicated that the cascade PID control strategy is applicable to the second-order time-delay plant that frequently suffers from secondary disturbances.

When the reference signal $r = 0$ and the primary secondary disturbance $d_1 = 1$ are considered as input conditions, the output responses y of the control systems Σ_{MCCS} and Σ_{SCS} are displayed in Fig. 12. The cascade PID controller reaches a smaller peak, which is more robust than
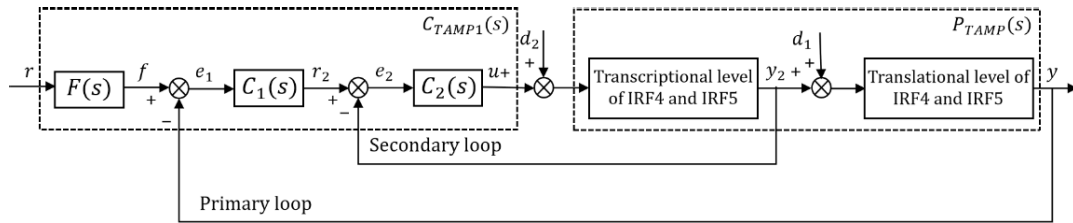
FIGURE 19. The cascade PID control strategy for IRF4 and IRF5 gene expression.

a single-loop PID controller in responding to the disturbances d_1. In fact, the primary disturbances occurring in the outer loop are transmitted to the inner loop by feedback, prompting the inner loop of the cascade control system to work for it.

The primary disturbance $d_1 = 1$ and secondary disturbance $d_2 = 1$ are assumed to simultaneously disrupt the SOPTD system which is the controlled plant of the control systems Σ_{MCCS} and Σ_{SCS}. According to the output response y shown in Fig. 13, it is observed that the cascade PID control system based on CRNs is less susceptible to disturbances d_1 and d_2 than the single-loop PID control system. Additionally, the cascade controller stabilizes the plant $P(s)$ at a faster rate.

Remark 4: This section simulates the CRN implementation of the cascade PID control system. As shown in Fig. 10-Fig. 13, the control system Σ_{MCCS} faster suppresses the disturbance signal than the control system Σ_{SCS} based on CRNs, since the manipulated variable y_2 of the controlled process is fed into the secondary loop and regulated by the secondary controller. Notably, the cascade PID control strategy significantly eliminates the secondary disturbance.

IV. THE FEASIBILITY OF CASCADE PID CONTROL SYSTEMS BASED ON DSD

The catalysis, degradation, and annihilation reactions in the CRNs are realized by the DSD reaction modules, which allow the equivalent mapping of the CRNs of a cascade PID control system to DSD reaction networks. In this part, a DSD technology-based cascade PID controller is further verified by Visual DSD.

Taking the CRNs of (20a)-(20h), (22a)-(22e), and (28a)-(28g) as templates, the DSD implementation of three essential chemical reactions is assembled as the cascade PID control system Σ_{MCCS}. In order to approximate as accurately as possible, the concentrations of all auxiliary species are kept at C_{max} to guarantee an adequate reaction with the input species. The reaction rate $q_t = k/C_{max}$ of a toehold t is determined by the number of bases, where k is the reaction rate of the desired chemical reaction. A degree of complementarity $c \in (0, 1)$ is introduced to ensure that $q_t c$ is much smaller than q_t without changing the toehold t, which is achieved by mismatching. For instance, DNA single strand T binds to the DNA double-strand complex G at a speed of $q_t c$ in the DSD implementation of the degradation reaction
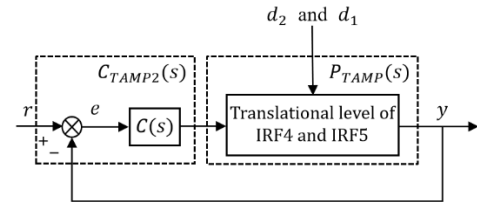

FIGURE 20. The single-loop PID control strategy for IRF4 and IRF5 gene expression.

depicted in Fig. 14. This allows degradation reactions to be significantly slower than annihilation reactions without the need for a redesign of toehold t.

Example 3: In an effort to validate the reliability of the DSD reactions-based cascade PID control system, a simulation experiment is performed. In addition to the cascade PID controller, a single-loop PID controller [10] is established for comparison. In this simulation, c and C_{max} are set to 0.00008 and 10000 nM, respectively. The concentrations of single-stranded DNA as the signal species are initialized to 0 nM. The remaining parameters are described in Table 6.

The simulation comparing control systems Σ_{MCCS} and Σ_{SCS}. investigates the following four representative cases: In Case 1, the reference input r is given by a square wave signal, and the perturbation inputs are assigned as 0. Under the condition of secondary disturbance $d_2 = 10^{-6}$ nM, Case 2 requires that the output y track the step signal $r = 10^{-6}$ nM steadily. When the primary disturbance of 10^{-6} nM occurs in the second-order time-delay biochemical process, the output response y of the control systems is analyzed in Case 3. Case 4 assumes the reference input $r = 10^{-6}$ nM, the primary disturbance $d_1 = 10^{-6}$ nM and the secondary disturbance $d_2 = 10^{-6}$ nM.

In order to explore the set-point tracking capability and long-term computational performance of the control system, a square wave signal is fed into the cascade PID controller and single-loop PID controller in Case 1. As seen in Fig. 15, the outputs y of the control systems Σ_{MCCS} and Σ_{SCS} track the square wave signal all the time. The difference is that the cascade PID control strategy exhibits a smooth response curve without overshoot.

The anti-disturbance ability of the DSD-based cascade PID control system is discussed in Cases 2, 3 and 4. Case 2 focuses

TABLE 8. Parameters of the control systems Σ_{TAMP1} and Σ_{TAMP2} for TAMs polarization process in Example 4.
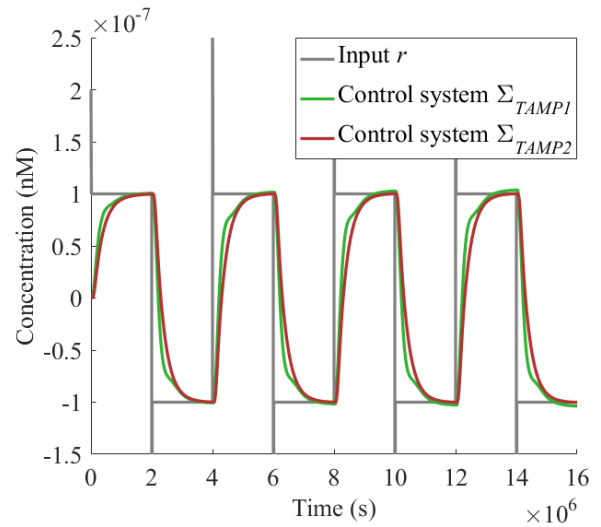
Control system Σ_{TAMP1}	Control system Σ_{TAMP2}
$C_{TAMP1}(s) \begin{cases} F(s)\{q_f = 0.028 \\ C_1(s) \begin{cases} q_{o1} = 2.856 \\ q_{o2} = 0.008 \\ q_{o3} = 0.361 \\ q_{o4} = 0.181 \end{cases} \\ C_2(s) \begin{cases} q_{i1} = 3.389 \\ q_{i2} = 0.042 \end{cases} \end{cases}$	$C_{TAMP2}(s) \begin{cases} q_1 = 3.389 \\ q_2 = 8.34 \times 10^{-3} \\ q_3 = 0.073 \\ q_4 = 0.037 \end{cases}$
$P_{TAMP}(s) \begin{cases} P_2(s) \begin{cases} q_{i3} = 10^{-5} \\ q_{i4} = 10^{-5} \\ q_{i5} = 4 \times 10^{-4} \\ q_{i6} = 2 \times 10^{-4} \end{cases} \\ P_1(s) \begin{cases} q_{o5} = 10^{-5} \\ q_{o6} = 10^{-5} \\ q_{o7} = 1.6 \times 10^{-3} \\ q_{o8} = 8 \times 10^{-4} \end{cases} \end{cases}$	$P_{TAMP}(s) \begin{cases} P_2(s) \begin{cases} q_{i3} = 10^{-5} \\ q_{i4} = 10^{-5} \\ q_{i5} = 4 \times 10^{-4} \\ q_{i6} = 2 \times 10^{-4} \end{cases} \\ P_1(s) \begin{cases} q_{o5} = 10^{-5} \\ q_{o6} = 10^{-5} \\ q_{o7} = 1.6 \times 10^{-3} \\ q_{o8} = 8 \times 10^{-4} \end{cases} \end{cases}$

TABLE 9. Overshoot of control systems Σ_{TAMP1} and Σ_{TAMP2} Based on DSD in response to the disturbances.
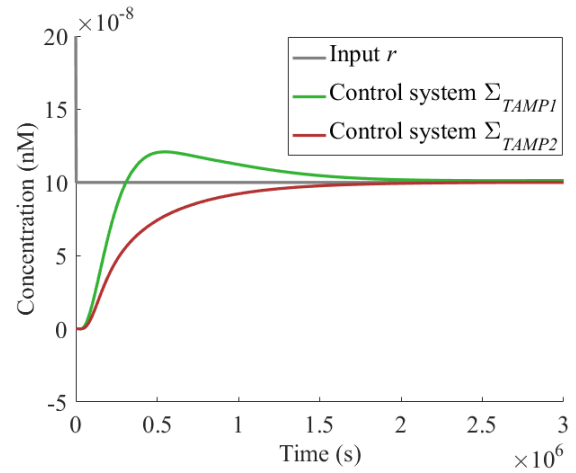
Disturbance input	Overshoot δ_O (%) of Σ_{TAMP1}	Overshoot δ_O (%) of Σ_{TAMP2}
$d_1 = 0, d_2 = 10^{-7}$	0	20.881
$d_1 = 10^{-7}, d_2 = 0$	6.669	18.07
$d_1 = 10^{-7}, d_2 = 10^{-7}$	6.072	52.687

FIGURE 21. Given a square wave signal r, the output trajectories of control systems Σ_{TAMP1} and Σ_{TAMP2}.

FIGURE 22. The output y of the control systems Σ_{TAMP1} and Σ_{TAMP2} in response to the internal disturbance $d_2 = 10^{-7}$ nM and reference signal $r = 10^{-7}$ nM.

on the suppression effect of the cascade PID controller on the secondary disturbance, so the input conditions of $r = 0$ nM, $d_2 = 10^{-6}$ nM and $d_1 = 0$ nM are considered. In contrast to the single-loop PID control system, the cascade PID control system has a faster settling time $t_s = 2901$ s, as shown in Fig. 16. Given a primary disturbance $d_1 = 10^{-6}$ nM in Case 3, the robustness of the two control systems is illustrated in Fig. 17. Obviously, the control system Σ_{MCCS} responds to the disturbance more quickly for avoiding a larger overshoot, indicating that the inner loop of the cascade control system is still effective for primary disturbances. Case 4 studies the responses of the control systems Σ_{MCCS} and Σ_{SCS} while the secondary disturbance $d_2 = 10^{-6}$ nM and the primary disturbance $d_1 = 10^{-6}$ nM coexist. There is no dispute in Fig. 18 that the cascade PID control method excellently and quickly attenuates disturbances d_1 and d_2. Table 7 details the overshoot of the control systems Σ_{MCCS} and Σ_{SCS} in Cases 2, 3 and 4.

Remark 5: This part constructs and simulates a cascade PID controller based on the DSD reaction. Table 7 lists the overshoot of the DSD-based control systems Σ_{MCCS} and Σ_{SCS} for different disturbance input conditions. These data demonstrate that the control system Σ_{MCCS} can significantly reduce and rapidly remove the impact of primary and secondary disturbances on the process $P(s)$.

V. THE CASCADE PID CONTROL STRATEGY FOR THE REGULATION OF TAMS POLARIZATION

The DSD-based cascade PID controller developed in this paper has broad application prospects. An example that regulates the polarization of TAMs by controlling the gene expression of IRF4 and IRF5 is given to demonstrate the applicability of the control strategy to a second-order biochemical system with time delay.

TAMs have the ability to repolarize, which is determined by the levels of IRF4 and IRF5 gene expression. IRF5 and IRF4 contribute to TAMs polarizing into the M1 phenotype that suppresses tumor growth and the M2 phenotype that encourages tumor development. Furthermore, IRF5 and IRF4 gene expression processes are represented by the
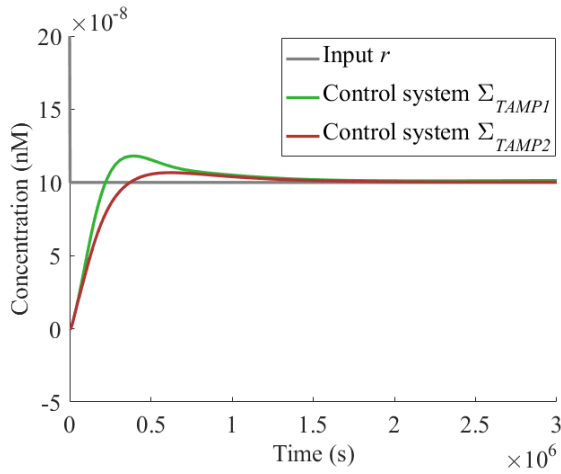
FIGURE 23. Under the condition of external disturbance $d_1 = 10^{-7}$ nM, the response of control systems Σ_{TAMP1} and Σ_{TAMP2} for the reference input r.
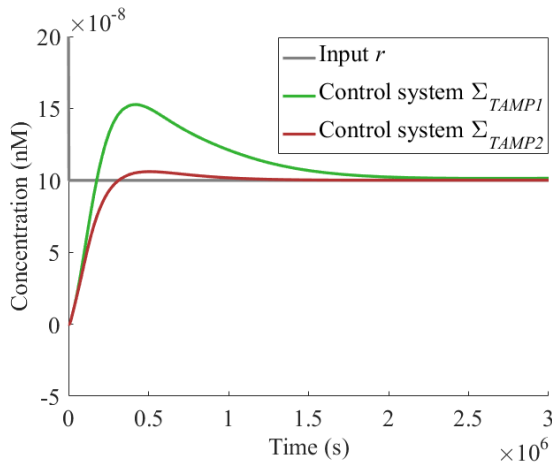
FIGURE 24. For the internal disturbance of $d_2 = 10^{-7}$ nM and the external disturbance of $d_1 = 10^{-7}$ nM, the responses of the control systems Σ_{TAMP1} and Σ_{TAMP2} to the input signal $r = 10^{-7}$ nM.

following reactions:

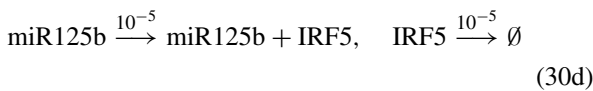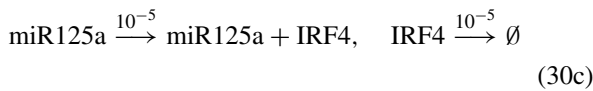$$\emptyset \xrightarrow{10^{-5}} \text{miR125a}, \quad \text{miR125a} \xrightarrow{10^{-5}} \emptyset \quad (30a)$$

$$\emptyset \xrightarrow{10^{-5}} \text{miR125b}, \quad \text{miR125b} \xrightarrow{10^{-5}} \emptyset \quad (30b)$$

$$\text{miR125a} \xrightarrow{10^{-5}} \text{miR125a} + \text{IRF4}, \quad \text{IRF4} \xrightarrow{10^{-5}} \emptyset \quad (30c)$$

$$\text{miR125b} \xrightarrow{10^{-5}} \text{miR125b} + \text{IRF5}, \quad \text{IRF5} \xrightarrow{10^{-5}} \emptyset \quad (30d)$$

$$\text{IRF4} + \text{IRF5} \xrightarrow{0.01} \emptyset \quad (30e)$$

It can be found in (30a)-(30e) that IRF4 and IRF5 are catalyzed by miR125a and miR125b, while the drop in the concentrations of all these species is dependent on annihilation and degradation reactions.

When the influence of the external environment is considered, the time delay caused by pH attracts attention. Thus, the process model of the above gene expression is

$$P_{TAMP}(s) = \frac{e^{-5 \times 10^4 s}}{10^{10} s^2 + 2 \times 10^5 s + 1} = \frac{e^{-10^4 s}}{10^5 s + 1} \frac{e^{-4 \times 10^4 s}}{10^5 s + 1} \quad (31)$$

Some other uncertain factors from the external environment hinder the ideal expression of the gene, such as gene overexpression resulting in superfluous gene products miR125a and miR125b and endogenous gene expression leading to redundant gene products IRF4 and IRF5. To this end, the disturbances encountered during transcription and translation of IRF4 and IRF5 gene expression need to be eliminated by control strategies. The regulation of the above gene expressions can be synchronized in a control system since the dual-rail representation adopted for the CRNS design means that each signal denotes a pair of species.

Example 4: As shown in Fig. 19, the secondary and primary loops of the cascade PID control system Σ_{TAMP1} regulate the transcription and translation of genes IRF4 and IRF5, respectively. Additionally, a single-loop PID control system Σ_{TAMP2} is constructed in Fig. 20 and used for comparison. The parameters of the control systems Σ_{TAMP1} and Σ_{TAMP2} are illustrated in Table 8.

The primary task of the control systems is to maintain the gene expression of IRF5 and IRF4 at the desired level. For this purpose, the output responses of the control systems Σ_{TAMP1} and Σ_{TAMP2} are considered for various input conditions. First, step changes are proposed to test the ability of the two control strategies to track the reference signal in the absence of disturbance. Then IRF5 gene overexpression, an internal perturbation of $d_2 = 10^{-7}$ nM, occurs during transcription. Next, external perturbation $d_1 = 10^{-7}$ nM caused by the cellular endogenous gene expression disturb IRF5 gene expression. Finally, the IRF5 and IRF4 gene expression is simultaneously subjected to internal perturbation $d_2 = 10^{-7}$ nM and external perturbation $d_1 = 10^{-7}$ nM. The above cases are simulated by Visual DSD and displayed in Fig. 21-Fig. 24.

In Fig. 21, the expression level of the IRF5 gene is requested to track the given square wave signal. Significantly, the cascade PID control system always reaches a steady state with a flatter curve. Additionally, the control system Σ_{TAMP1} runs steadily at all times. However, the control system Σ_{TAMP2} drifts and overshoots gradually, which is attributed to the consumption of DNA fuel species. When IRF5 gene overexpression affects the transcriptional process, in Fig. 22, the control system Σ_{TAMP1} stabilizes with no overshoot. The cascade PID controller still has an advantage against the disturbance from endogenous gene expression, as shown in Fig. 23, because the external disturbance in the primary loop enters the secondary loop via feedback. As can be observed in Fig. 24, the gene expression of IRF4 and IRF5 is effectively controlled by a cascade PID control scheme under the condition of $d_1 = 10^{-7}$ nM and $d_2 = 10^{-7}$ nM.

For different perturbations, a comparison between control systems Σ_{TAMP1} and Σ_{TAMP2} in terms of overshoot δ_o is indicated in Table 9. Crucially, IRF5 gene expression is barely affected by gene overexpression that is promptly eliminated in the secondary loop.

Remark 6: The cascade control method (Fig. 19) and single-loop control method (Fig. 20) are proposed for the TAMs polarization process by regulating the gene expression of IRF4 and IRF5. As shown in Fig. 21-Fig. 24, control system Σ_{TAMP1} ensures that the production of IRF5 is maintained at a satisfactory level when the overexpression of the gene and the expression of the endogenous gene result in an excess of the gene products miRNA125b and IRF5. In short, the cascade PID control strategy is capable of eliminating internal perturbations encountered by the transcription process and rejecting external perturbations experienced by the translation process.

VI. CONCLUSION

The cascade PID control system is constructed by utilizing DSD reactions and is applied to regulate TAMs polarization in this manuscript. First, the CRN and DSD are employed to realize a cascade PID controller and a second-order time-delay process. The derived controller quickly and effectively suppresses the internal and external disturbances suffered by the second-order time-delay biochemical system. Then, a first-order low-pass filter is coupled with the cascade PID control system to modify the reference signal delivered to the cascade PID controller. The filter works well to keep cascaded primary and secondary controllers from generating excessive control signals and unwanted overshoots in responding to the reference input signal. Finally, a DSD-based cascade PID control method is adopted to regulate IRF4 and IRF5 gene expression associated with the polarization process of tumor-associated macrophages. Even if gene overexpression disturbs the transcription process and endogenous gene expression perturbs the translation process, the cascade PID control strategy proposed in this work guarantees IRF4 and IRF5 gene expression at the desired level. Future work will devote efforts to the biochemical realization of more controllers, such as linear quadratic regulator controllers.

NOMENCLATURE
NOTATION

|	
C_1	Primary controller.
C_2	Secondary controller.
C_{CCS}	Cascade PID controller.
C_{MCCS}	Modified cascade PID controller.
C_{SCS}	Single-loop PID controller.
d_1 and d_2	Primary disturbance and secondary disturbance.
F	First-order low-pass filter.
P_1	Primary process.
P_2	Secondary process.
r, e_1, and y	The reference signal, error signal, and output signal of the outer loop.
r_2, e_2, and y_2	The reference signal, error signal, and output signal of the inner loop.
Σ_{CCS}	Cascade control system.
Σ_{MCCS}	Modified cascade control system.
Σ_{SCS}	Single-loop control system.

ACRONYMS

CCS	Cascade control system.
CRNs	Chemical reaction networks.
DSD	DNA strand displacement.
FOPTD	First order plus time delay.
IRF4	Interferon regulatory factor 4.
IRF5	Interferon regulatory factor 5.
MCCS	Modified cascade control system.
SCS	Single-loop control system.
SOPTD	Secondary order plus time delay.
TAMs	Tumor-associated macrophages.

REFERENCES

[1] R. Alexander, G. Campani, S. Dinh, and F. V. Lima, "Challenges and opportunities on nonlinear state estimation of chemical and biochemical processes," *Processes*, vol. 8, no. 11, p. 1462, Nov. 2020.

[2] F. Meng and T. Ellis, "The second decade of synthetic biology: 2010–2020," *Nature Commun.*, vol. 11, no. 1, p. 5174, Oct. 2020.

[3] A. Patel and S. Sen, "Computational framework for design of a pulse generating biomolecular circuit," *IFAC-PapersOnLine*, vol. 53, no. 1, pp. 220–225, 2020.

[4] E. Zhu, C. Chen, Y. Rao, and W. Xiong, "Biochemical logic circuits based on DNA combinatorial displacement," *IEEE Access*, vol. 8, pp. 34096–34103, 2020.

[5] W. Zhong and J. T. Sczepanski, "Direct comparison of D-DNA and L-DNA strand-displacement reactions in living mammalian cells," *ACS Synth. Biol.*, vol. 10, no. 1, pp. 209–212, Jan. 2021.

[6] J. P. Unsleber and M. Reiher, "The exploration of chemical reaction networks," *Annu. Rev. Phys. Chem.*, vol. 71, no. 1, pp. 121–142, Apr. 2020.

[7] C. Zou, X. Wei, Q. Zhang, and Y. Liu, "Synchronization of chemical reaction networks based on DNA strand displacement circuits," *IEEE Access*, vol. 6, pp. 20584–20595, 2018.

[8] K. Oishi and E. Klavins, "Biomolecular implementation of linear I/O systems," *IET Syst. Biol.*, vol. 5, no. 4, pp. 252–260, Jul. 2011.

[9] R. Sawlekar, F. Montefusco, V. V. Kulkarni, and D. G. Bates, "Implementing nonlinear feedback controllers using DNA strand displacement reactions," *IEEE Trans. Nanobiosci.*, vol. 15, no. 5, pp. 443–454, Jul. 2016.

[10] N. M. G. Paulino, M. Foo, J. Kim, and D. G. Bates, "PID and state feedback controllers using DNA strand displacement reactions," *IEEE Control Syst. Lett.*, vol. 3, no. 4, pp. 805–810, Oct. 2019.

[11] M. Whitby, L. Cardelli, M. Kwiatkowska, L. Laurenti, M. Tribastone, and M. Tschaikowski, "PID control of biochemical reaction networks," *IEEE Trans. Autom. Control*, vol. 67, no. 2, pp. 1023–1030, Feb. 2022.

[12] H. Lv, Q. Li, J. Shi, C. Fan, and F. Wang, "Biocomputing based on DNA strand displacement reactions," *ChemPhysChem*, vol. 22, no. 12, pp. 1151–1166, 2021.

[13] C. Chen, J. Wen, Z. Wen, S. Song, and X. Shi, "DNA strand displacement based computational systems and their applications," *Frontiers Genet.*, vol. 14, Feb. 2023, Art. no. 1120791.

[14] Y. Yuan, H. Lv, and Q. Zhang, "Molecular device design based on chemical reaction networks: State feedback controller, static pre-filter, addition gate control system and full-dimensional state observer," *J. Math. Chem.*, vol. 60, no. 5, pp. 915–935, May 2022.

[15] Y. Yuan, H. Lv, and Q. Zhang, "DNA strand displacement reactions to accomplish a two-degree-of-freedom PID controller and its application in subtraction gate," *IEEE Trans. Nanobiosci.*, vol. 20, no. 4, pp. 554–564, Oct. 2021.

[16] Y. Li, H. Lv, and X. Wang, "The design of 2DOF IMC-PID controller in biochemical reaction networks," *Appl. Sci.*, vol. 13, no. 6, p. 3402, Mar. 2023.

[17] I. Kaya, N. Tan, and D. P. Atherton, "Improved cascade control structure for enhanced performance," *J. Process Control*, vol. 17, no. 1, pp. 3–16, 2007.

[18] A. Campos-Rodríguez, J. P. García-Sandoval, V. González-Álvarez, and A. González-Álvarez, "Hybrid cascade control for a class of nonlinear dynamical systems," *J. Process Control*, vol. 76, pp. 141–154, Apr. 2019.

[19] M. A. Siddiqui, M. N. Anwar, S. H. Laskar, and M. R. Mahboob, "A unified approach to design controller in cascade control structure for unstable, integrating and stable processes," *ISA Trans.*, vol. 114, pp. 331–346, Aug. 2021.

[20] S. Pashaei and P. Bagheri, "Parallel cascade control of dead time processes via fractional order controllers based on Smith predictor," *ISA Trans.*, vol. 98, pp. 186–197, Mar. 2020.

[21] C. Wang, H. Sun, and Q. Zhao, "Improved cascade control system for a class of unstable processes with time delay," *Int. J. Control, Automat. Syst.*, vol. 17, no. 1, pp. 126–135, 2019.

[22] N. Wang and X. Pan, "Path following of autonomous underactuated ships: A translation–rotation cascade control approach," *IEEE/ASME Trans. Mechatronics*, vol. 24, no. 6, pp. 2583–2593, Dec. 2019.

[23] Z. Sun, G. Pritschow, P. Zahn, and A. Lechler, "A novel cascade control principle for feed drives of machine tools," *CIRP Ann.*, vol. 67, no. 1, pp. 389–392, 2018.

[24] A. Zoukit, H. Doubabi, I. Salhi, and N. Abdenouri, "Advanced cascade control strategy applied to an indirect hybrid solar-gas dryer: Numerical and experimental investigations," *Sustain. Energy Technol. Assess.*, vol. 53, Oct. 2022, Art. no. 102380.

[25] W. Zhang, C. Ma, H. Li, L. Xuan, and A. An, "DMC-PID cascade control for MEA-based post-combustion CO_2 capture process," *Chem. Eng. Res. Design*, vol. 182, pp. 701–713, Jun. 2022.

[26] L. Wang, T. Feng, J. Song, Z. Guo, and J. Hu, "Model checking optimal infinite-horizon control for probabilistic gene regulatory networks," *IEEE Access*, vol. 6, pp. 77299–77307, 2018.

[27] M. H. Khammash, "Cybergenetics: Theory and applications of genetic control systems," *Proc. IEEE*, vol. 110, no. 5, pp. 631–658, May 2022.

[28] C. L. Kelly, A. W. K. Harris, H. Steel, E. J. Hancock, J. T. Heap, and A. Papachristodoulou, "Synthetic negative feedback circuits using engineered small RNAs," *Nucleic Acids Res.*, vol. 46, no. 18, pp. 9875–9889, Oct. 2018.

[29] X. Xiang, J. Wang, D. Lu, and X. Xu, "Targeting tumor-associated macrophages to synergize tumor immunotherapy," *Signal Transduction Targeted Therapy*, vol. 6, no. 1, p. 75, Feb. 2021.

[30] J. Gao, Y. Liang, and L. Wang, "Shaping polarization of tumor-associated macrophages in cancer immunotherapy," *Frontiers Immunology*, vol. 13, Jun. 2022, Art. no. 888713.

[31] Q. Chang, Y. Hao, Y. Wang, Y. Zhou, H. Zhuo, and G. Zhao, "Bone marrow mesenchymal stem cell-derived exosomal microRNA-125a promotes M2 macrophage polarization in spinal cord injury by downregulating IRF5," *Brain Res. Bull.*, vol. 170, pp. 199–210, May 2021.

[32] A. Hu, X. Chen, Q. Bi, Y. Xiang, R. Jin, H. Ai, and Y. Nie, "A parallel and cascade control system: Magnetofection of miR125b for synergistic tumor-association macrophage polarization regulation and tumor cell suppression in breast cancer treatment," *Nanoscale*, vol. 12, no. 44, pp. 22615–22627, 2020.

[33] B. Yordanov, J. Kim, R. L. Petersen, A. Shudy, V. V. Kulkarni, and A. Phillips, "Computational design of nucleic acid feedback control circuits," *ACS Synth. Biol.*, vol. 3, no. 8, pp. 600–616, Aug. 2014.
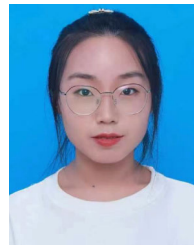
HUIHUI XUE received the B.E. degree in software engineering from the Business College of Shanxi University, in 2020. She is currently pursuing the master's degree in software engineering with Dalian University. Her research interests include biochemical reaction networks, DNA strand displacement reactions, and molecular controllers.

HUI LV received the B.S. and M.S. degrees in applied mathematics from Liaoning University, Shenyang, China, in 2004 and 2009, respectively, and the Ph.D. degree in control theory and control engineering from Northeastern University, Shenyang, in 2015.

She is currently an Associate Professor with the Key Laboratory of Advanced Design and Intelligent Computing, Ministry of Education, Dalian University, Dalian, China. Her research interests include DNA computing, biochemical reaction networks, and hybrid control systems.
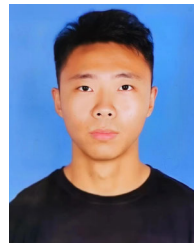
YIJUN XIAO received the B.E. degree in medical information engineering from Jining Medical University, in 2020. He is currently pursuing the master's degree in computer science and technology with Dalian University. His research interests include biochemical reaction networks and molecular controller.

XING'AN WANG received the B.S. degree in materials physics from Harbin Engineering University, Harbin, China, in 2000, the M.S. degree in materials science from Guizhou University, Guiyang, China, in 2010, and the Ph.D. degree in materials science from the Harbin Institute of Technology, Harbin, in 2017.

He is currently a Lecturer with the Liaoning Engineering Laboratory of Special Optical Functional Crystals, College of Environmental and Chemical Engineering, Dalian University, Dalian, China. His research interests include nanochemistry, numerical simulation calculation, and functional materials.

• • •